Modeling of Coupled Dome-Shaped Microoscillators

Tuhin Sahai and Alan T. Zehnder

***Abstract*—Synchronized micromechanical oscillators have potential for applications in signal processing, neural computing, sensing, and other fields. This paper explores the conditions under which coupled nonlinear limit cycle microoscillators can synchronize. As an example of the modeling approach and to be able to obtain results for a system that has been experimentally realized, thermally excited dome oscillators, which are fabricated by buckling of a thin circular film of polysilicon, are modeled. Starting with the von Kármán plate equations and an assumed mode shape, a Galerkin projection is performed to obtain an ordinary differential equation for the postbuckled dynamics of the mode. Because the structure is thermally excited, a thermal model is built by solving the heat equation on a disk with appropriate boundary conditions. Bifurcation analysis of the single oscillator model is performed to look for basic underlying phenomena. Conditions under which two slightly detuned coupled limit cycle dome oscillators will synchronize are explored. [2007-0208]**

***Index Terms*—Buckling, coupled oscillators, Galerkin projections, resonators, thermomechanical modeling.**

I. Introduction

MICROMECHANICAL oscillators have been an active area of research in the last decade with the promise of numerous applications [1]. They display a rich range of behavior that is rarely seen in macroscopic structures. Examples include multiple parametric resonances [2], [3], optically driven limit cycles [4], entrainment [5], tunability [6], and super- and subharmonic resonances [2], [7]. These devices are thus very interesting both for basic [8]–[10] and applied research in areas such as sensing [11]–[14], signal processing [15], reference oscillators [16], and pattern recognition [17]. Their small size and low damping couple these structures with the actuation and detection mechanisms in complicated ways, giving rise to nonlinear phenomena [4], [5], [18]. In addition, MEMS oscillators can be coupled to each other, leading to potential applications such as neurocomputers [17], filters, and means of clock distribution in microprocessors.

It is also possible to construct digital memory elements using MEMS oscillators. The underlying idea is to synchronize multiple oscillators with different phase relationships. Each oscillator potentially becomes a single "bit" of data. Fig. 1 shows a schematic of the overall setup. Here, the master oscillator is not influenced by the other oscillators and is free to vibrate. The other oscillators (slaves) are coupled to the master oscillator.

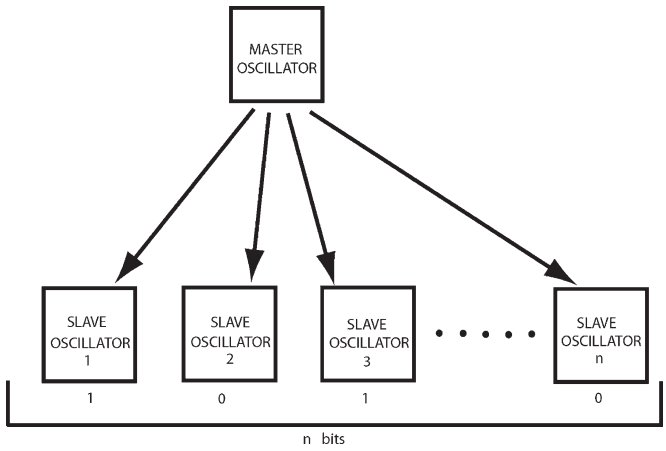

Fig. 1. Schematic denoting data storage using MEMS oscillators.

Let the equation for the motion of each (slave) oscillator be (using the same form as in [17])

$$m\ddot{x}_i + f(x_i, \lambda_i)\dot{x}_i + g(x_i) = \zeta_i \dot{x}_s \qquad \forall i = 1, \ldots, n. \quad (1)$$

Assuming velocity coupling of the slave oscillator to the master, m is the mass of the oscillator, x_i is the state of the ith oscillator, and ζ_i is the strength of electrical coupling between the master and slave. ζ_i has a real and imaginary part, giving $\zeta_i = p_i e^{i\psi_i}$, and x_s is the state of the master oscillator, which is governed by

$$m\ddot{x}_s + f(x_s, \lambda_s)\dot{x}_s + g(x_s) = 0. \quad (2)$$

This equation is of the same form as (1) with an omitted coupling term.

Averaging the governing equations and neglecting the amplitude equation give [17]

$$\dot{\theta}_i = \omega_i + p_i \sin(\theta_s - \theta_i + \psi_i) \quad (3)$$

where θ_s denotes the phase of oscillation of the master oscillator, and θ_i and ω_i denote the phase and frequency of oscillation of the ith slave. p_i is a measure of coupling between the ith slave and master, and ψ_i is a measure of phase introduced by the coupling. The averaged phase equation of the master is

$$\dot{\theta}_s = \omega_s \quad (4)$$

Manuscript received August 21, 2007; revised April 2, 2008. This work was supported in part by the Cornell Center for Materials Research, in part by the Materials Research Science and Engineering Center of the National Science Foundation under Grant DMR-0520404, and in part by the National Science Foundation under Grant CMS 0600174. Subject Editor G. Fedder.

T. Sahai was with the Department of Theoretical and Applied Mechanics, Cornell University, Ithaca, NY 14853 USA. He is now with the United Technologies Research Center, East Hartford, CT 06108 USA (e-mail: ts269@cornell.edu).

A. T. Zehnder is with the Department of Theoretical and Applied Mechanics and the Sibley School of Mechanical and Aerospace Engineering, Cornell University, Ithaca, NY 14853 USA.

Color versions of one or more of the figures in this paper are available online at http://ieeexplore.ieee.org.

Digital Object Identifier 10.1109/JMEMS.2008.924844

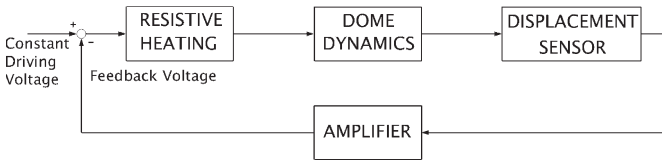

Fig. 2. Block diagram of the proposed scheme to construct thermally driven MEMS limit cycle oscillators.

where ω_s is the frequency of oscillation of the master. Let $\chi_i = \theta_i - \theta_s$

$$\dot{\chi}_i = \omega_i - \omega_s + p_i \sin(-\chi_i + \psi_i). \tag{5}$$

If ζ_i in (1) is real, it follows that $\psi_i = 0$. The governing equation has equilibria at the following:

$$\chi_{i0} = \sin^{-1}\left(\frac{\omega_s - \omega_i}{p_i}\right) \tag{6}$$

$$\chi_{i0} = \sin^{-1}\left(\frac{\omega_s - \omega_i}{p_i}\right) + \pi. \tag{7}$$

If $p_i > 0$, then equilibrium 1 given by (6) is stable. If $p_i < 0$, then equilibrium 2 given by (7) becomes stable. By flipping the sign of the electrical coupling, one can switch the phase of the entrained oscillators, thus toggling the bit. A potential advantage of such systems over standard memory storage devices is the speed of data access. MEMS resonators can oscillate at frequencies in several hundreds of megahertz [8], thus potentially giving rise to very fast memory elements.

This paper focuses on the dynamics of two coupled dome-shaped MEMS oscillators. The aim is to study the conditions under which coupled limit cycle microoscillators synchronize with each other. In this paper, mechanical and electrothermal coupling are considered.

To illustrate the basic phenomena associated with coupled MEMS oscillators and to study a system that has been experimentally realized, we have chosen to model thermally excited dome oscillators. The domes are fabricated by first depositing a thin film of polysilicon onto a silicon dioxide layer [15], [19]. The deposition parameters are tuned to ensure that the polysilicon is under a large (approximately 220 MPa) residual compressive stress. A circular region of the oxide layer is then etched away, leaving a thin precompressed circular disk that buckles into a shallow dome. Although domes of various sizes can be made, a typical oscillator has a diameter of 10 to 40 μm.

In the experiments by Reichenbach *et al.* [15], the dome was driven by resistive heating and the motion was optically detected. Because it may be difficult to integrate the optical detection of motion into commercial applications, a different detection mechanism is preferred. A capacitive displacement sensor or strain gauges fabricated onto the surface of the oscillator could be used. We envision a system in which the output of the displacement sensor is fed back to a resistive heater fabricated onto the oscillator (see Fig. 2). The coupling between the motion of the oscillator and temperature will give rise to the limit cycle oscillations seen in [15].

Before studying the synchronization of coupled microoscillators, let us first understand the dynamics of one oscillator.

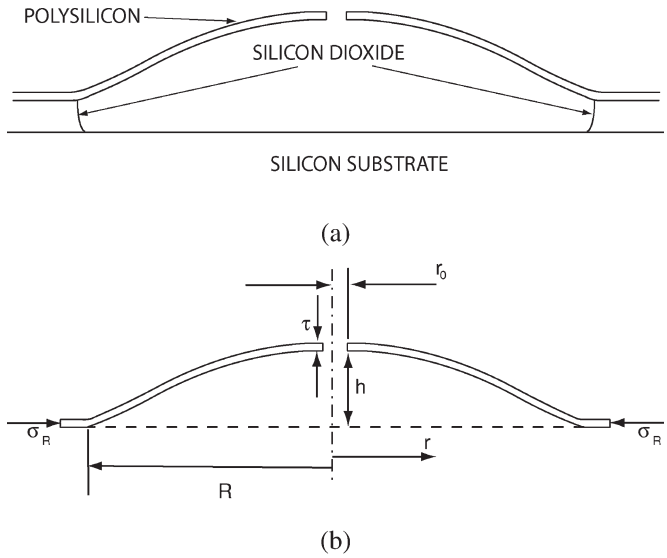

Fig. 3. Schematics of the dome oscillator. (a) Schematic cross section of axisymmetric dome oscillator. (b) Coordinates and parameters of the dome oscillator.

A set of nonlinear ordinary differential equations (ODEs) that model the governing dynamics of a single mode of oscillation of the dome is derived. The method can be used to build models of various oscillators; however, as an example, consider a particular dome with an outer diameter of 40 μm, inner diameter of 4 μm, height of 1 μm, and thickness of 200 nm.

II. Modeling of a Single Dome Oscillator

A. Mechanical Model Using Galerkin Projection

To study the dynamics of the oscillator, an ODE model for oscillations of the dome about the buckled state is constructed. After the disk buckles into a shallow dome, its shape will be as shown in Fig. 3. The postbuckled shape is approximated by the following:

$$w(r) = \frac{1 - \cos\left(\frac{\pi(r-R)}{R}\right)}{2} \tag{8}$$

where r is the radial distance measured from the center of the dome [see Fig. 3(b)] and R is the outer radius of the dome oscillator ($R = 20$ μm). The shape function $w(r)$ satisfies the zero deflection and zero slope boundary conditions $w(R) = 0$ and $w'(R) = 0$, respectively, and monotonically decreases with increasing r. However, $w(r)$ does not satisfy the moment-free boundary condition

$$M_{rr} = \frac{d^2 w(r)}{dr^2} + \frac{\nu}{r}\frac{dw(r)}{dr} = 0 \tag{9}$$

on the hole edge $r = r_0$ (ν in the aforementioned equation is the Poisson's ratio). Efforts to find a simple function that would satisfy all boundary and monotonicity conditions were not successful. However, comparisons of FEM solutions of a dome with and without a hole show that the overall error incurred by violating the $M_{rr} = 0$ condition on the hole is minor.

It is assumed that the mode shape of oscillation is the same as that of the buckling shape (8). Hence, the time dependent oscillations of the dome can be expressed as

$$u(r,t) = A(t)w(r) = A(t)\frac{\left(1-\cos\left(\frac{\pi(r-R)}{R}\right)\right)}{2} \tag{10}$$

where $A(t)$ is the amplitude of oscillation. To obtain an ODE for oscillation about the buckled state, perform a Galerkin projection [20] on the governing partial differential equation (PDE) similar to the calculation for beams in [21]. The projection yields an ODE for the assumed mode of vibration. This ODE will have equilibria that physically correspond to the buckled state of the plate. The coordinates are transformed to describe vibrations of the oscillator about the buckled equilibria.

The nonlinear von Kármán equations [20] that couple the in-plane stretching of the plate to its out-of-plane bending are used to describe the motion. The dynamic von Kármán equations for axisymmetric problems reduce to

$$\nabla^4\phi(r,t) = E\frac{1}{r}\frac{\partial^2 u(r,t)}{\partial r^2}\frac{\partial u(r,t)}{\partial r} \tag{11}$$

$$\rho\tau\frac{\partial^2 u(r,t)}{\partial t^2} + \gamma\frac{\partial u(r,t)}{\partial t} + D_m\nabla^4 u(r,t) = -\frac{1}{r}\left[\frac{\partial\phi(r,t)}{\partial r}\frac{\partial^2 u(r,t)}{\partial r^2} + \frac{\partial^2\phi(r,t)}{\partial r^2}\frac{\partial u(r,t)}{\partial r}\right] \tag{12}$$

where u is the deflection of the plate, ϕ is the stress function, $\nabla^4 = (1/r)(\partial/\partial r)r(\partial/\partial r)(1/r)(\partial/\partial r)r(\partial/\partial r)$, and $D_m = E\tau^3/(12(1-\nu^2))$. In the aforementioned equation, E, ρ, and ν are the Young's modulus, density, and Poisson's ratio, respectively, τ is the thickness of the oscillator, and γ is the damping.

Using $u(r,t)$ from (10), we solve (11) for $\phi(r,t)$. Successively integrating (11) yields

$$\phi(r,t) = (A(t))^2\left[\tilde{f}\left(\mathrm{ci}\left(\frac{2\pi r}{R}\right), \cos\left(\frac{2\pi r}{R}\right), \ln\left(\frac{2\pi r}{R}\right), r\right)\right] + C_1\ln(r) + C_2 r^2 + C_3 r^2\ln(r) \tag{13}$$

where $\mathrm{ci}(x) = -\int_x^\infty(\cos(t)/t)dt$ and f is a nonlinear function determined by successive integration. Take $C_3 = 0$ in the complementary solution to keep the displacement field single valued [22]. The constants C_1 and C_2 are determined by imposing stress boundary conditions. The boundary condition at $r = r_0$ is $\sigma_r = 0$ and, at $r = R$, is $\sigma_r = \sigma_R$. This translates into $(1/r_0)(\partial\phi(r,t)/\partial r)|_{r=r_0} = 0$ and $(1/R)(\partial\phi(r,t)/\partial r)|_{r=R} = \sigma_R$.

A Galerkin projection is performed by solving

$$\int_{r_0}^{R}\left[\rho\tau\frac{\partial^2 u(r,t)}{\partial t^2} + \gamma\frac{\partial u(r,t)}{\partial t} + D_m\nabla^4 u(r,t) + \frac{1}{r}\times\left[\frac{\partial\phi(r,t)}{\partial r}\frac{\partial^2 u(r,t)}{\partial r^2} + \frac{\partial^2\phi(r,t)}{\partial r^2}\frac{\partial u(r,t)}{\partial r}\right]\right]\times w(r)dr = 0 \tag{14}$$

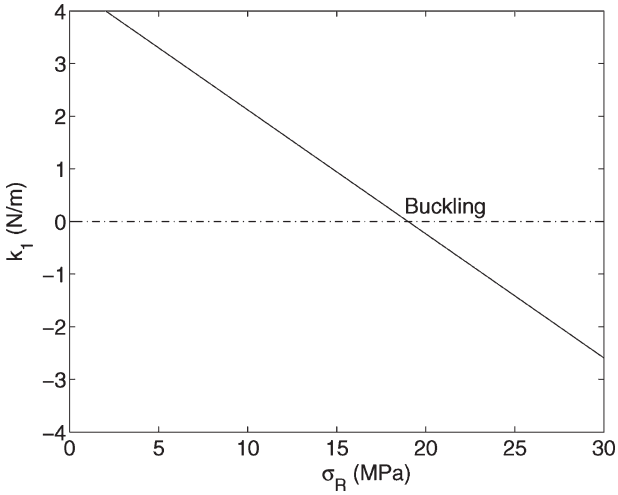

Fig. 4. Variation of linear stiffness of the plate with applied compressive stress.

to obtain an ODE for $A(t)$, physically constraining the dynamics of the oscillator to the mode given by (8). The solution to $\phi(r,t)$ is substituted into (14). The presence of terms such as $\mathrm{ci}(2\pi r/R)$ and $\ln(2\pi r/R)$ complicate the integration for the Galerkin projection; however, these two terms can be approximated by using 4×4 Padé approximants [23]. $m\times n$ Padé approximations involve the approximation of the original function with the rational functions of the form

$$P_m^n(x) = \frac{\sum_{i=0}^n L_i x^i}{\sum_{j=0}^m N_j x^j}. \tag{15}$$

The coefficients L_i and N_j are calculated to give the best approximation to the original function [23].

Using the procedure outlined previously, the Galerkin projection yields an ODE for motion of the oscillator

$$m\ddot{A}(t) + \gamma'\dot{A}(t) + k_1 A(t) + k_3 A(t)^3 = 0 \tag{16}$$

where $m = \rho\tau\int_{r_0}^R w(r)^2 dr$, $\gamma' = \gamma\int_{r_0}^R w(r)dr$, and k_1 and k_3 are the linear and cubic stiffnesses, respectively, calculated by using the Galerkin projection procedure described previously. The stiffness k_1 is found to be a linear function of σ_R, which is the radial stress at the outer edge of the disk, as shown in Fig. 4. The cubic stiffness, however, is independent of σ_R. The value of σ_R at which $k_1 = 0$ is the buckling load. For the dimensions and properties of our problem, the critical buckling stress is found to be $\sigma_R \approx 19$ MPa. This compares well with the theoretical value of 21 MPa [24] for a circular plate of the same dimensions with no hole. For $\sigma_R > 19$ MPa, $k_1 < 0$ and the structure assumes a buckled shape with equilibrium displacement given by $A^\star = \pm\sqrt{-k_1/k_3}$. The experimentally observed deflection of the dome is ≈ 1 μm [19], which corresponds to $\sigma_R \approx 62$ MPa. Thus, the stress release due to buckling reduces the in-plane radial stress σ_R from 220 to $\approx$62 MPa.

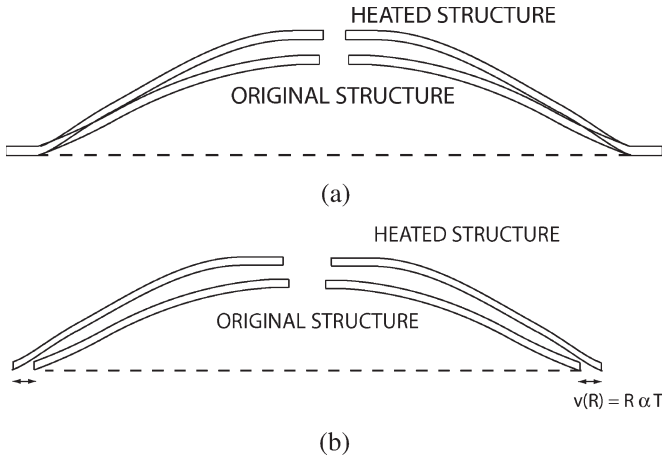

Fig. 5. Schematics of the effect of heat on the dome oscillator. (a) Schematic of dome oscillator with and without heating. (b) Hypothetical thermal expansion of oscillator in the absence of constraints.

B. Thermal Stress Effects

We consider oscillators driven thermally via resistive heaters fabricated onto the device. Temperature change will induce thermal stresses in the dome, changing stiffness, and will result in thermal expansion, causing additional upward deflection [see Fig. 5(a)]. Use a superposition approach in which the dome is allowed to freely expand when heated by a temperature T (above ambient). Then, the radial boundary stress σ_R is increased to negate the radial displacement in the free expansion. The stiffness and deflection of the dome at this new stress level can then be computed. Although the temperature distribution would depend on the heater layout details, the average temperature of the structure is used.

To calculate the change in σ_R, first, compute the radial displacement at $r = R$ due to compressive stress σ_R applied on $r = R$. From the von Kármán theory [20], the radial strain is

$$\epsilon_r = \frac{\partial v(r)}{\partial r} + \frac{1}{2}\frac{\partial u(r)}{\partial r} = \frac{\sigma_r - \nu\sigma_\theta}{E} \tag{17}$$

where $v(r)$ is the radial displacement field and $u(r)$ is the out-of-plane displacement (10). Using the stress function $\phi(r,t)$ (13), $\sigma_R = \sigma_r(r = R)$ and $\sigma_\theta(r = R)$ are calculated, and (17) is integrated to obtain $v(r)$ in terms of σ_R. Linearizing about the 62-MPa compressive stress needed to cause the 1-μm deflection, a linear relation between $v(R)$ and σ_R can be obtained.

Assuming a free thermal expansion of $v(R) = \alpha RT$, where α is the coefficient of thermal expansion (see Table I), the stress increment $\Delta\sigma_R$ needed to push the boundary back by $v(R) = -\alpha RT$ can be calculated from the linear relation between $v(R)$ and σ_R. Thus, the dependence of the boundary stress on temperature can be written as

$$\sigma_R = \sigma_0 + \eta T \tag{18}$$

where σ_0 is the 62-MPa boundary stress at ambient temperature and the coefficient η relating the temperature change to the change in stress has a value, by the previously described procedure, of 0.146 MPa/K.

TABLE I
MATERIAL PROPERTIES OF POLYSILICON [25], [26]

E	160 GPa
ρ	2330 $\frac{kg}{m^3}$
α	$2.6 \times 10^{-6}/K$
k	20 $\frac{W}{mK}$
C_p	753 $\frac{J}{kgK}$
ν	0.22

As the temperature changes, increasing σ_R, the linear stiffness k_1 changes, thus we denote it as $k_1(T)$. If k_1 changes, the equilibrium of (16) $A^\star(T) = \sqrt{-k_1(T)/k_3}$ shifts upwards. In addition, the temperature change causes the dome to expand upwards even if σ_R were not increased.

The net effect is that

$$\text{Change in height} = A^\star(T)\alpha\Delta T + A^\star(T + \Delta T) - A^\star(T). \tag{19}$$

The first term captures the increase in height due to free thermal expansion, and the next two terms account for the shift in equilibrium due to stiffness change. Linearizing

$$\text{Change in height} \approx D'T \tag{20}$$

where D' can be approximated by the following:

$$D' = A^\star(T)\alpha + \frac{dA^\star(T)}{dT}. \tag{21}$$

The aforementioned can be collected to build a model for the dome oscillator that includes the effect of thermal strains. Moving the origin in (16) to the buckled state for convenience

$$x(t) = A(t) - A^\star(0) \tag{22}$$

yields

$$m\ddot{x}(t) + \gamma'\dot{x}(t) - 2k_1(T)x(t) + 3\sqrt{-k_1(T)k_3}x(t)^2 + k_3x(t)^3 = 0. \tag{23}$$

Recall that $k_1(T) < 0$ in the postbuckled state. This equation still neglects the thermal deflection $\approx D'T$ due to temperature change. We will treat the thermal deflection as a base motion by transforming the equation with $\chi(t) = x(t) + D'T$. By dividing the equation by m, nondimensionalizing time $t = \omega_0\xi$ and deflection by the thickness of the oscillator $z = \chi(t)/\tau$, the system becomes

$$\ddot{z} + \frac{(\dot{z} - D\dot{T})}{Q} + h(T)(z - DT) + 3\sqrt{\frac{h(T)\beta}{2}}\tau(z - DT)^2 + \beta(z - DT)^3 = 0 \tag{24}$$

where $\omega_0 = \sqrt{-2k_1(0)/m}$. Because we know how the linear stiffness in terms of σ_R and how σ_R changes with T, we can calculate $h(T)$ in terms of T to give $h(T) = 1 + 0.00023T$. Calculations on height increase give $D = D'/\tau \approx 6 \times 10^{-4}$ K.

From the Galerkin projection, $\beta \approx 0.5$. The quality factor Q of the device is experimentally found to be ≈ 2500 [19].

III. Thermal Modeling of a Single Dome Oscillator

A. Temperature Field

To complete the model, an ODE that captures the thermal dynamics of the structure is needed. A simple analysis shows that cooling occurs essentially due to conduction; radiation and convective cooling are found to play a negligible role. Thus, let us start with the axisymmetric heat equation given by the following:

$$\frac{\partial T(r,t)}{\partial t} = a\left[\frac{\partial^2 T(r,t)}{\partial r^2} + \frac{1}{r}\frac{\partial T(r,t)}{\partial r}\right] + q \qquad (25)$$

where $T(r,t)$ is the temperature field above ambient, a is thermal diffusivity, and q is the uniform thermal flux (applied to the entire dome) due to resistive heating. In practice, resistive heating may act nonuniformly on the oscillator. However, detailed FEM simulations performed for a similar device [27] predict that the resulting thermal stresses are well approximated by those that would arise from an equivalent uniform temperature.

The thermal diffusivity $a = k/\rho C_p$, where k is the thermal conductivity, ρ is the density, and C_p is the specific heat of polysilicon (see Table I). The calculated value of a based on Table I is 0.114 cm^2/s. An experimentally measured value of $a = 0.165$ cm^2/s corresponding to a thermal conductivity value of $k = 29$ W/mK can be found in [28]. There is some uncertainty in which the value of a should be used. Here, we use the calculated value, noting that the two values are close.

To solve (25), break the solution $T(r,t)$ into two parts

$$T(r,t) = T_{\rm tr}(r,t) + T_{\rm ss}(r). \qquad (26)$$

$T_{\rm tr}(r,t)$ is the transient heat solution, and $T_{\rm ss}(r)$ is the steady state solution. Assuming that at $t = 0$ the disk is at room temperature, the initial condition is $T(r,0) = 0$. The boundary conditions are $T(R,t) = 0$ and $\partial T(r_0,t)/\partial r = 0$ (no heat flux at r_0) (see Fig. 6). The heat equation (25) with the assumed solution (26) gives

$$\frac{\partial T_{\rm tr}(r,t)}{\partial t} = a\left[\frac{\partial^2 T_{\rm tr}(r,t)}{\partial r^2} + \frac{1}{r}\frac{\partial T_{\rm tr}(r,t)}{\partial r}\right] + a\left[\frac{\partial^2 T_{\rm ss}(r)}{\partial r^2} + \frac{1}{r}\frac{\partial T_{\rm ss}(r)}{\partial r}\right] + q. \qquad (27)$$

The steady state part of the solution must satisfy

$$a\left[\frac{d^2 T_{\rm ss}(r)}{dr^2} + \frac{1}{r}\frac{dT_{\rm ss}(r)}{dr}\right] + q = 0. \qquad (28)$$

The solution to (28) is of the form

$$T_{\rm ss}(r) = -\frac{qr^2}{4a} + B_1 \ln(r) + B_2. \qquad (29)$$

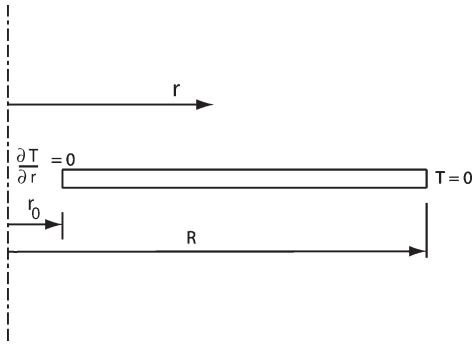

Fig. 6. Cross section of the heated disk with boundary conditions.

$B_1 = qr_0^2/2a$ and $B_2 = (qR^2/4a) - (qr_0^2/2a)\ln(R)$ from boundary conditions. Therefore

$$T_{\rm ss}(r) = \frac{q(R^2 - r^2)}{4a} + \frac{qr_0^2}{2a}\left(\ln(r) - \ln(R)\right). \qquad (30)$$

From the initial condition, we know that $T_{\rm ss}(r) + T_{\rm tr}(r,0) = 0$. This implies that $T_{\rm tr}(r,0) = -T_{\rm ss}(r)$, where $T_{\rm ss}(r)$ is given in (30). Now, solve for $T_{\rm tr}(r,t)$ given by the following:

$$\frac{\partial T_{\rm tr}(r,t)}{\partial t} = a\left[\frac{\partial^2 T_{\rm tr}(r,t)}{\partial r^2} + \frac{1}{r}\frac{\partial T_{\rm tr}(r,t)}{\partial r}\right]. \qquad (31)$$

Following the steps in [29] for a similar problem, let $T_{\rm tr}(r,t) = e^{-a\mu^2 t}G(r)$ to obtain

$$\frac{d^2 G(r)}{dr^2} + \frac{1}{r}\frac{dG(r)}{dr} + \mu^2 G(r) = 0. \qquad (32)$$

This is Bessel's equation of order zero with boundary conditions $dG(r_0)/dr = 0$ and $G(R) = 0$. The solution to the aforementioned equation is of the form

$$G(r) = A_1 J_0(\mu r) + A_2 Y_0(\mu r) \qquad (33)$$

where J_0 and Y_0 are zero-order Bessel functions of the first and second kind, respectively. From the boundary conditions

$$\begin{aligned} A_1 J_0(\mu R) + A_2 Y_0(\mu R) &= 0 \\ A_1 J_0'(\mu r_0) + A_2 Y_0'(\mu r_0) &= 0. \end{aligned} \qquad (34)$$

Using

$$G(r) = E_k\left(Y_0'(\mu r_0)J_0(\mu r) - J_0'(\mu r_0)Y_0(\mu r)\right) \qquad (35)$$

the condition of no heat flux at $r = r_0$ is trivially satisfied. E_k is an arbitrary nonzero constant. Now, from the condition at $r = R$, solve for μ

$$Y_0'(\mu r_0)J_0(\mu R) - J_0'(\mu r_0)Y_0(\mu R) = 0. \qquad (36)$$

Equation (36) has an infinite number of positive real roots $\mu_1, \mu_2, \ldots$ Rewrite $G(r)$ as $G(\mu r)$, corresponding to different μ's, and look for an expansion of the form

$$T_{\rm ss}(r) = D_1 G(\mu_1 r) + D_2 G(\mu_2 r) + D_3 G(\mu_3 r) + \cdots. \qquad (37)$$

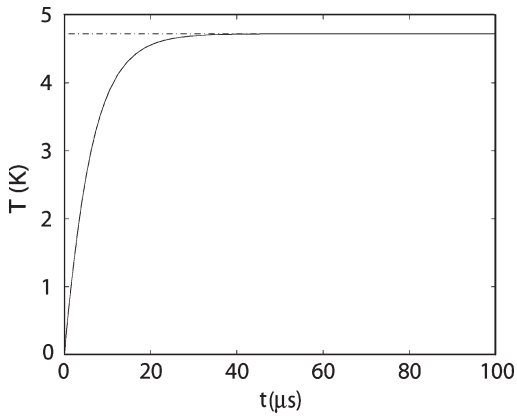

Fig. 7. Average temperature as a function of time at $r = r_0 = 2$ μm for $q = 1.14 \times 10^{-2}$ W/m^2.

It is known that $\int_{r_0}^{R} rG(\mu_i r)G(\mu_j r)dr = 0$ if $i \neq j$. Thus, $D_j = -(\int_{r_0}^{R} rT_{\rm ss}(r)G(\mu_j r)dr / \int_{r_0^R} rG(\mu_j r)^2 dr)$.

A value of $q = 1.14 \times 10^{-2}$ (a step function at $t = 0$) is picked for numerical ease (simplifies the fraction q/a), and the resulting $T_{\rm ss}(r)$ is fit with a Bessel expansion, as explained previously. A three-term Bessel expansion in (37) gives a reasonable approximation to $T_{\rm ss}(r)$. Thus, the temperature $T(r,t)$ can be written as follows:

$$T(r,t) = \frac{q(R^2 - r^2)}{4a} + \frac{qr_0^2}{2a}\left(\ln(r) - \ln(R)\right) + \sum_{i=0}^{\infty} D_i e^{-a\mu_i^2 t} G(\mu_i r). \quad (38)$$

B. Lumped Thermal Mass Model

The time history of temperature given by (38) can be calculated for any value of r. To simplify, consider the average temperature of the structure

$$T = \frac{\int_0^{2\pi}\int_{r_0}^{R} rT(r,t)drd\theta}{\pi\left(R^2 - r_0^2\right)} \quad (39)$$

where $T(r,t)$ is given by (38). The average temperature of the disk is shown as a function of time in Fig. 7. This response can be captured by Newton's law of cooling

$$\dot{T} = -B_T T + A_T P \quad (40)$$

where P is the total power input ($P = q \times$ area), A_T is the inverse of the lumped thermal mass of the structure, and B_T gives the rate of cooling due to conduction. The values of A_T and B_T can be obtained from the thermal response of the structure. Because $T(0) = 0$, we know that $\dot{T}(0) = A_T P$ and as $t \to \infty$ $T = A_T P/B$. Using these two relations, the values $A_T \approx 1.3 \times 10^{-3}$ K/μW and $B_T \approx 1.544 \times 10^{-1}$ are calculated. The thermal equation (40) is also rescaled in time by $t = \omega_0 \xi$ to make it consistent with (24).

C. Thermomechanical Feedback

The thermal aspect of the problem is not completely described by (40). As previously mentioned, to induce limit cycle oscillations, the motion of the device must be coupled to the heating by detecting by the displacement and feeding this signal into the resistive heating with the appropriate gain (Fig. 2). The power dissipated by resistive heating is $P_{\rm dissipated} = V^2/R$, where V is the voltage across the resistor and R is the resistance. Incorporating this quadratic relationship yields a new equation that governs the average thermal dynamics of the oscillator

$$\dot{T} = -B_T T + A_T P(1 + c_g z)^2. \quad (41)$$

Here, c_g is the feedback gain (see Fig. 2). $c_g = -2$ is selected for analysis, noting that c_g could be tuned to virtually any value.

IV. Bifurcation Analysis of the Model

Putting together the mechanical (24) and thermal (41) equations yields the thermomechanical system

$$\begin{aligned} &\dot{T} + B_T T - A_T P(1 + c_g z)^2 = 0 \\ &\ddot{z} + \frac{(\dot{z} - D\dot{T})}{Q} + h(T)(z - DT) \\ &\quad + 3\sqrt{\frac{h(T)\beta}{2}}\tau(z - DT)^2 + \beta(z - DT)^3 = 0. \end{aligned} \quad (42)$$

The equilibria of the system given by (42) can be computed. Only one real equilibrium exists and is given by $z = DT$ and $T = A_T P/B_T - c_g D A_T P$. For the constants quoted previously, $z = 6 \times 10^{-4}$ T, where $T = 0.0084P/1 - 5 \times 10^{-5} P$. This equilibrium is the new buckled state of the heated dome oscillator. The stability of this equilibrium can be determined by computing the Jacobian and its corresponding characteristic equation. It is found that, for $P < 3600$ μW, the equilibrium is stable. At $P \approx 3605$ μW, it loses stability. The results were checked by using the continuation software AUTO 2000 [30], [31]. Starting with the equilibrium at $P = 0$ μW ($z = 0$ and $T = 0$), the equilibrium with changing resistive heating (denoted by P) is computed, as shown in Fig. 8. In Fig. 8, the equilibrium loses stability at a supercritical Hopf bifurcation [32]. Using AUTO 2000 again, the limit cycles born at the Hopf bifurcation are tracked (Fig. 9).

V. Coupled Limit Cycle Oscillators

To force the dome oscillator into limit cycle oscillations, select $P = 3800$ μW. It is clear from Fig. 9(a) that, at $P = 3800$ μW, the maximum displacement of the dome, in one oscillation, is $z_{\max} \approx 0.2$ (or 0.2 $\times$ the thickness of the dome). Consider a pair of dome oscillators with different frequencies of oscillation detuned by $\sqrt{\kappa - 1}$. Effectively, manufacturing variabilities are lumped into κ. The question now posed is can the two oscillators be synchronized? If so, by what means? To address these questions, two different types of coupling are considered.

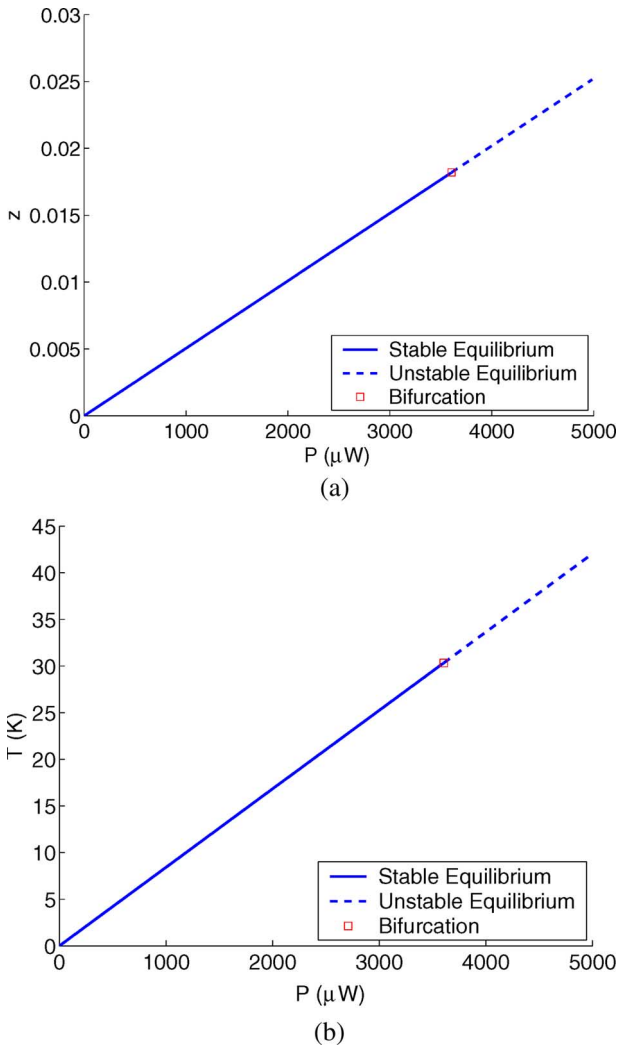

Fig. 8. Equilibrium point ($z = DT$) with increasing heat input (P). Obtained by using continuation algorithms.

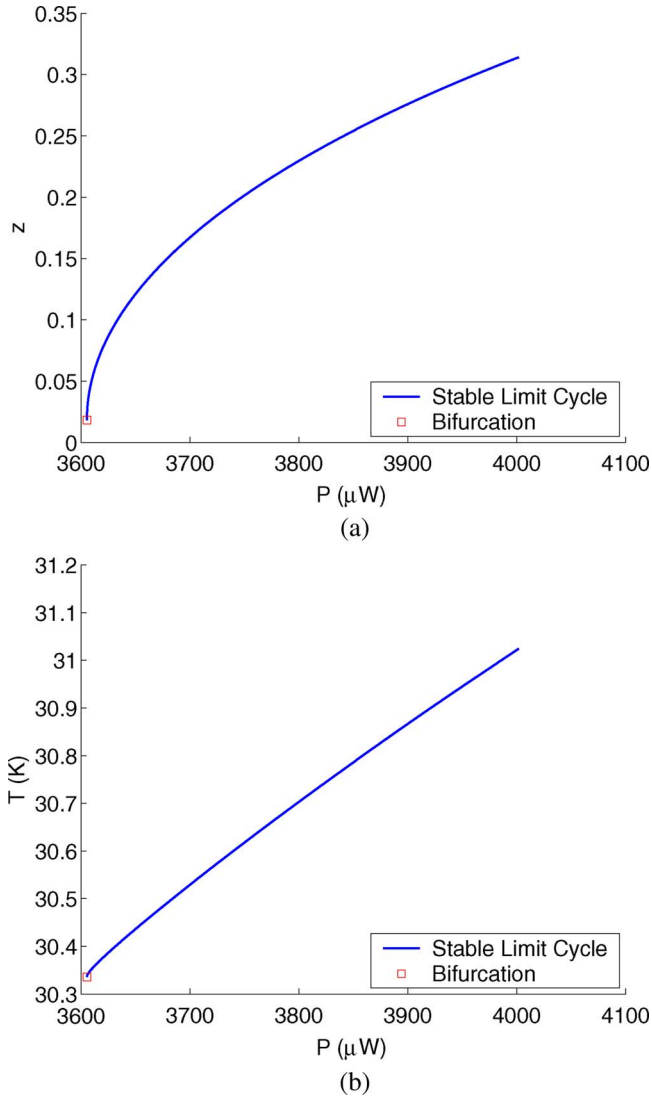

Fig. 9. Continuation of the limit cycles born at the Hopf bifurcation. (a) Maximum displacement versus input power. (b) Maximum temperature versus input power.

A. Mechanical Coupling

Mechanical coupling could be achieved by fabricating springs that connect multiple oscillators together [33]. These connecting springs drive each oscillator toward the state of the other oscillator. Two mechanically coupled oscillators can be modeled by using two versions of (42) with the addition of a linear spring term that couples the two oscillators

$$\begin{aligned}
&\dot{T}_1 + B_T T_1 - A_T P(1 + c_g z_1)^2 = 0 \\
&\ddot{z}_1 + \frac{(\dot{z}_1 - D\dot{T}_1)}{Q} + h_1(T_1)(z_1 - DT_1) \\
&\quad + 3\sqrt{\frac{h_1(T_1)\beta}{2}}\tau(z_1 - DT_1)^2 + \beta(z_1 - DT_1)^3 = K(z_2 - z_1) \\
&\dot{T}_2 + B_T T_2 - A_T P(1 + c_g z_2)^2 = 0 \\
&\ddot{z}_2 + \frac{(\dot{z}_2 - D\dot{T}_2)}{Q} + h_2(T_2)(z_2 - DT_2) \\
&\quad + 3\sqrt{\frac{h_2(T_2)\beta}{2}}\tau(z_2 - DT_2)^2 + \beta(z_2 - DT_2)^3 = K(z_1 - z_2)
\end{aligned} \tag{43}$$

where $h_1(T) = \kappa + cT_1$, $h_2(T) = 1 + cT_2$, $(T_1, z_1, \dot{z}_1)$ and $(T_2, z_2, \dot{z}_2)$ represent the states of the first and second oscillators, respectively, κ is a measure of detuning between the two oscillators (changing κ changes the frequency of the first oscillator), and K is the stiffness of the connecting spring relative to the linear stiffness of the dome at ambient temperature.

Numerical integration is used to compute the value of coupling stiffness needed to synchronize the two oscillators. Both oscillators start from the same initial condition for different values of detuning and coupling stiffnesses. After a prescribed amount of integration time ($\approx 4Q$ cycles), we check if the two oscillators are oscillating in synchrony. The ability to synchronize is mapped out by varying the relative coupling stiffness and detuning, resulting in that shown in Fig. 10. $\kappa = 1$ corresponds to identical oscillators and hence requires $K = 0$ to synchronize them. From Fig. 10, it is seen that, at $\kappa = 0.9$ (approximately 5% difference in frequency), a relative coupling stiffness of $K = 1$ is needed to achieve synchrony.

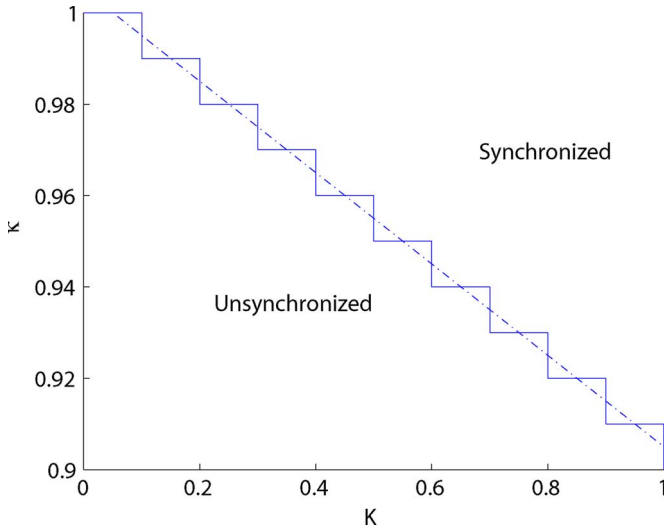

Fig. 10. Relative coupling stiffness versus detuned frequency of oscillator 1 required to achieve synchrony. The solid lines form steps due to the square grid used to compute the region of synchrony. The dotted line denotes the curve that the steps converge to on taking a finer and finer grid.

Even though mechanical coupling is possible (as shown in [33]) it may not be convenient because it involves additional fabrication steps, tuning is difficult, and coupling between arbitrary oscillators (that are not neighbors) is infeasible. Thus, let us consider a tunable method to electrothermally couple the dome oscillators.

B. Electrothermal Coupling

In this form of coupling, the motion of one oscillator is fed back as a driving voltage to the heater of the other (see Fig. 11). The model equations for this system are as follows:

$$\dot{T}_1 + B_T T_1 - A_T P(1 + c_g z_1 + \phi_c z_2)^2 = 0$$

$$\ddot{z}_1 + \frac{(\dot{z}_1 - D\dot{T}_1)}{Q} + h_1(T_1)(z_1 - DT_1) + 3\sqrt{\frac{h_1(T_1)\beta}{2}}\tau(z_1 - DT_1)^2 + \beta(z_1 - DT_1)^3 = 0$$

$$\dot{T}_2 + B_T T_2 - A_T P(1 + c_g z_2)^2 = 0$$

$$\ddot{z}_2 + \frac{(\dot{z}_2 - D\dot{T}_2)}{Q} + h_2(T_2)(z_2 - DT_2) + 3\sqrt{\frac{h_2(T_2)\beta}{2}}\tau(z_2 - DT_2)^2 + \beta(z_2 - DT_2)^3 = 0 \quad (44)$$

where ϕ_c is the tunable coupling strength. In this setup, oscillator 2 (master oscillator) has its own internal feedback loop (Fig. 2) but is not affected in any way by oscillator 1 (slave oscillator). Oscillator 1 sees a heater voltage that is equal to the displacement of oscillator 2, which is multiplied by coupling factor ϕ_c. To check for synchrony (entrainment [32]), sweep oscillator 2 in frequency by changing the parameter κ. Numerically integrate the system for $4Q$ cycles (to get rid of transients), and look at the response of oscillator 1. On sweeping forward in κ, it is found that the oscillator 1 entrains to the signal

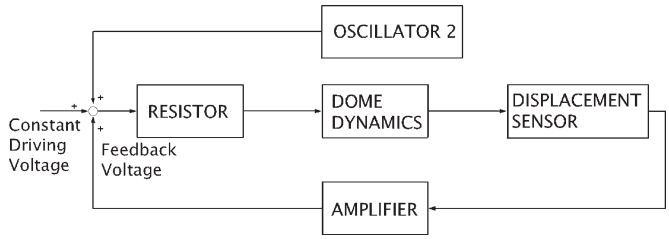

Fig. 11. Box diagram for electrically coupling dome oscillators.

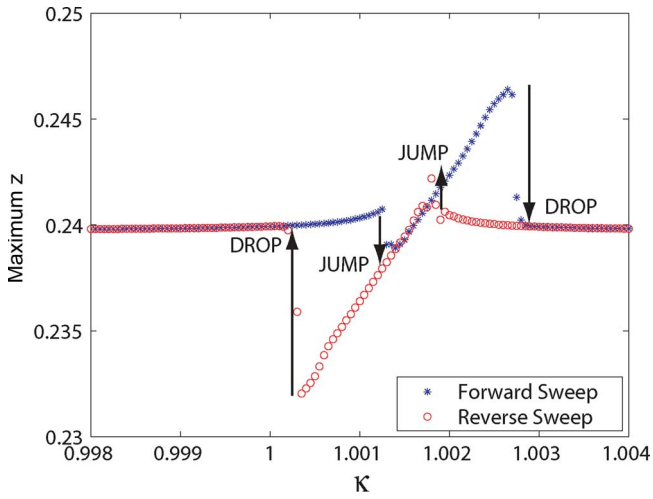

Fig. 12. Entrainment of oscillator 1 to the signal from oscillator 2. Detuning versus maximum amplitude for $\phi_c = 0.01$.

from oscillator 2 when the quasi-periodic motion jumps onto the backbone curve of oscillator 1 (see Fig. 12). The response then drops down from the top of the backbone curve onto the quasi-periodic motion (see Fig. 12). On sweeping back in κ, the quasi-periodic motion loses stability and oscillator 1 entrains to the signal from oscillator 2 by jumping onto the backbone curve. On sweeping κ further down, the entrained solution loses stability and the system drops to the quasi-periodic motion. The locations of the jumps and drops change on changing the coupling coefficient ϕ_c. By computing the jumps and drops for a range of values of ϕ_c, the entrainment regions are shown in Fig. 13.

The curves in Fig. 13 are the locations of jumps and drops in forward and reverse sweeps. The region inside the V-shaped structures is the region of entrainment (different for different directions of sweeping). The entire region slopes to the right because the $(1 + c_g z_1 + \phi_c z_2)^2$ term has a nonzero average, which increases with ϕ_c. This, in turn, increases the average temperature of oscillator 1, detuning the location of the resonance curve to the right (caused by the $h_1(T) = 1 + cT_1$ term). Similar jumps and drops have been found in mushroom-shaped MEMS oscillators, which are optically and mechanically excited [34], [35]. The phase difference between the two oscillators is shown in Fig. 14. The phase difference depends on the direction of sweeping. On the forward sweep, the slave oscillator locks into the master oscillator at a phase difference above $\pi/2$. On sweeping forward in detuning, the phase reduces. Eventually, the phase difference reduces to $\approx \pi/6$, and

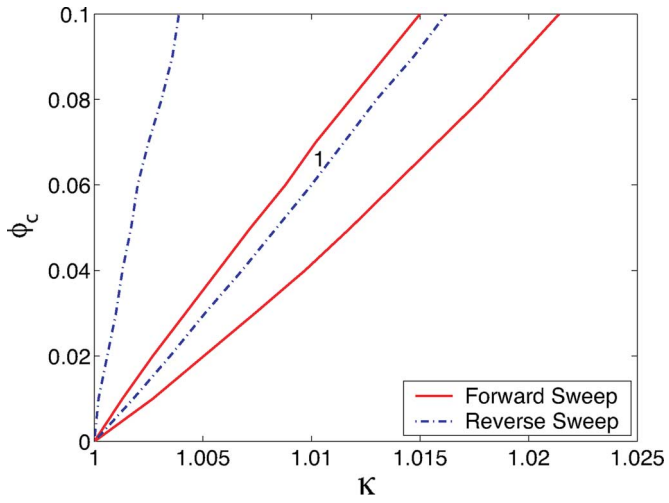

Fig. 13. Detuning versus coupling parameter. Oscillators synchronize inside the V-shaped structure. Different curves denote regions of entrainment for forward and reverse sweeps. Solid line: Forward sweep. Dotted line: Reverse sweep. The region denoted by 1 is the overlap of the entrainment regions due to forward and backward sweeps.

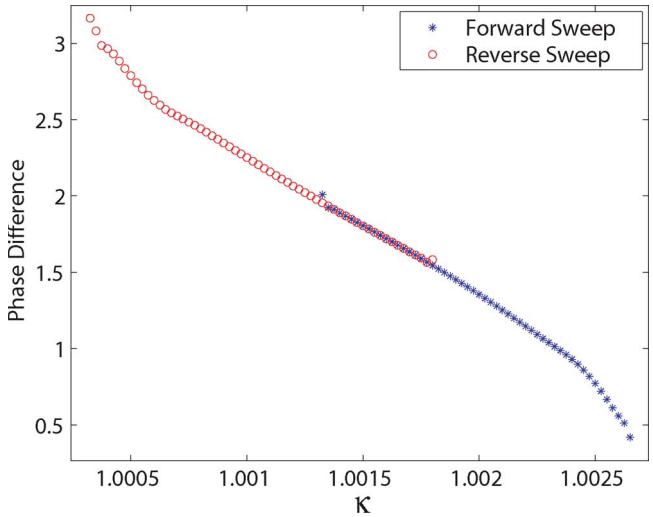

Fig. 14. Phase difference between oscillators (during entrainment) versus detuning for $\phi_c = 0.01$.

the oscillator drops out of the entrainment region. On sweeping down in detuning, the system locks in at a phase difference of $\approx\pi/2$. On sweeping down further, the phase difference increases to $\approx\pi$ at which point the slave oscillator is not entrained to the master. This method of coupling can be used to construct memory elements mentioned previously. The "on" and "off" bits are slave oscillators that are either in or out of synchrony with the master. Thus, by sweeping in the coupling ϕ_c, one can change the phase difference between the two oscillators that can be used to construct the memory elements shown in Fig. 1. For $\phi_c < 0$, we get the same region as shown in Fig. 13, except that it is reflected about the x- and y-axes. The region then lies in the third quadrant (in the space of detuning and coupling). The phase on sweeping through the entrainment regions for $\phi_c < 0$ is shown in Fig. 15. The figure is similar to Fig. 14 with an addition of π.

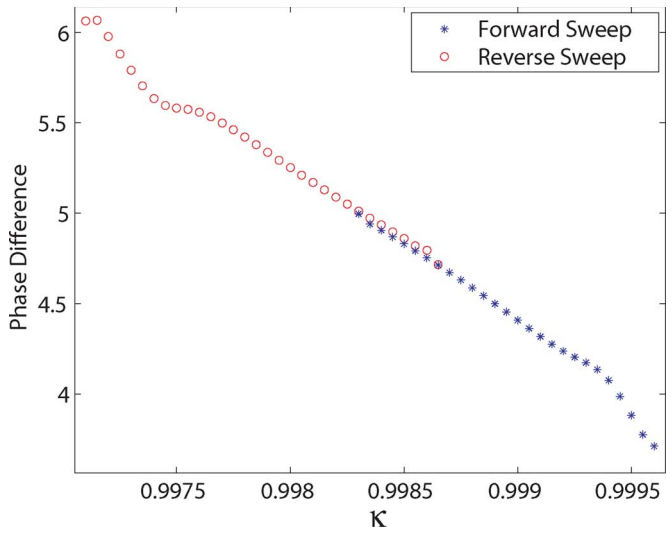

Fig. 15. Phase difference between oscillators (during entrainment) versus detuning for $\phi_c = -0.01$.

VI. Conclusion

This paper analyzes how a system of synchronized coupled oscillators might be designed, constructed, and implemented. In this paper, dome-shaped oscillators are used as an example. A model is constructed by starting from the governing PDE and performing a Galerkin projection to obtain an ODE for a chosen mode of oscillation. The domes are actuated by using a resistive heating element, and the motion is fed back into the actuation, driving the dome oscillators into limit cycles with the proper choice of feedback gain. A model for the thermal characteristics of the dome is constructed by solving the heat equation on an annulus, yielding an ODE that governs the average thermal response of dome-shaped microoscillators. The effect of heating on the stresses and thermal expansion of the structure is included to give a complete governing set of ODEs. A bifurcation analysis of the 3-D ODE system is performed to find limit cycle oscillations. By driving two detuned dome oscillators into limit cycle oscillations, the conditions under which they synchronize are explored. Both mechanical and electrical methods of coupling are found, under the right conditions, to successfully synchronize/entrain the two oscillators in frequency. Future work could include careful bifurcation analysis of the coupled dome oscillators using numerical and perturbative techniques, study of the behavior of an array of oscillators, and incorporation of noise into the system.

Acknowledgment

The authors would like to thank T. Healey for the valuable discussions and suggestions.

References

[1] T. Sahai and A. Zehnder, "Modeling and dynamics of coupled dome-shaped micromechanical oscillators," in *Proc. NSTI Conf. Nanotechnol. Trade Show*, 2007, pp. 77–80.

[2] K. Turner, S. Miller, P. Hartwell, N. MacDonald, S. Strogatz, and S. Adams, "Five parametric resonances in a microelectromechanical system," *Nature*, vol. 396, no. 6707, pp. 149–152, Nov. 1998.

[3] M. Yu *et al.*, "Realization of parametric resonances in a nanowire mechanical system with nanomanipulation inside a scanning electron microscope," *Phys. Rev. B, Condens. Matter*, vol. 66, no. 7, p. 073 406, Aug. 2002.
[4] K. Aubin, M. Zalalutdinov, T. Alan, R. Reichenbach, R. Rand, A. Zehnder, J. Parpia, and H. Craighead, "Limit cycle oscillations in CW laser-driven NEMS," *J. Microelectromech. Syst.*, vol. 13, no. 6, pp. 1018–1026, Dec. 2004.
[5] M. Zalalutdinov, K. Aubin, M. Pandey, A. Zehnder, R. Rand, H. Craighead, and J. Parpia, "Frequency entrainment for micromechanical oscillator," *Appl. Phys. Lett.*, vol. 83, no. 16, pp. 3281–3283, Oct. 2003.
[6] M. Zalalutdinov, B. Ilic, D. Czaplewski, A. Zehnder, H. Craighead, and J. Parpia, "Frequency-tunable micromechanical oscillator," *Appl. Phys. Lett.*, vol. 77, no. 20, pp. 3287–3289, Nov. 2000.
[7] V. Kaajakari and A. Lal, "Parametric excitation of circular micromachined polycrystalline silicon disks," *Appl. Phys. Lett.*, vol. 85, no. 17, pp. 3923–3925, Oct. 2004.
[8] H. Craighead, "Nanoelectromechanical systems," *Science*, vol. 290, no. 5496, pp. 1532–1535, Nov. 2000.
[9] X. M. H. Huang, C. A. Zorman, M. Mehregany, and M. L. Roukes, "Nanoelectromechanical systems: Nanodevice motion at microwave frequencies," *Nature*, vol. 421, no. 6922, p. 496, Jan. 2003.
[10] A. Watson, "Getting the measure of nanotechnology," *Science*, vol. 306, no. 5700, pp. 1309–1310, Nov. 2004.
[11] J. S. Aldridge and A. N. Cleland, "Noise-enabled precision measurements of a duffing nanomechanical resonator," *Phys. Rev. Lett.*, vol. 94, no. 15, p. 156 403, Apr. 2005.
[12] B. Ilic, H. C. D. Czaplewski, P. Neuzil, C. Campagnolo, and C. Batt, "Mechanical resonant immunospecific biological detector," *Appl. Phys. Lett.*, vol. 77, no. 3, pp. 450–452, Jul. 2000.
[13] K. Ekinci, X. Huang, and M. Roukes, "Ultrasensitive nanoelectromechanical mass detection," *Appl. Phys. Lett.*, vol. 84, no. 22, pp. 223–256, May 2004.
[14] A. Cleland and M. L. Roukes, "A nanometre-scale mechanical electrometer," *Nature*, vol. 392, no. 6672, pp. 160–162, Mar. 1998.
[15] R. Reichenbach, M. Zalalutdinov, K. Aubin, R. Rand, B. Houston, J. Parpia, and H. Craighead, "Third-order intermodulation in a micromechanical thermal mixer," *J. Microelectromech. Syst.*, vol. 14, no. 6, pp. 1244–1252, Dec. 2005.
[16] S. Lee, M. Demirci, and C. Nguyen, "A 10-MHz micromechanical resonator Pierce reference oscillator for communications," in *Dig. Tech. Papers, 11th Transducers*, 2001, pp. 1094–1097.
[17] F. Hoppensteadt and E. M. Izhikevich, "Synchronization of MEMS resonators and mechanical neurocomputing," *IEEE Trans. Circuits Syst. I, Fundam. Theory Appl.*, vol. 48, no. 2, pp. 133–138, Feb. 2001.
[18] T. Sahai, R. Bhiladvala, and A. Zehnder, "Thermomechanical transitions in doubly-clamped micro-oscillators," *Int. J. Non-linear Mech.*, vol. 42, no. 4, pp. 596–607, May 2007.
[19] M. Zalalutdinov, K. Aubin, R. Reichenbach, A. Zehnder, B. Houston, J. Parpia, and H. Craighead, "Shell-type micromechanical actuator and resonator," *Appl. Phys. Lett.*, vol. 83, no. 18, pp. 3815–3817, Nov. 2003.
[20] Y. C. Fung, *Foundations of Solid Mechanics*, 1st ed. Englewood Cliffs, NJ: Prentice-Hall, 1965.
[21] P. Holmes and J. Marsden, "A partial differential equation with infinitely many periodic orbits: Chaotic oscillations of a forced beam," *Arch. Ration. Mech. Anal.*, vol. 76, no. 2, pp. 135–165, Jun. 1981.
[22] S. Timoshenko and J. Goodier, *Theory of Elasticity*, 3rd ed. New York: McGraw-Hill, 1970.
[23] C. M. Bender and S. A. Orszag, *Advanced Mathematical Methods for Scientists and Engineers I*, 1st ed. New York: Springer-Verlag, 1999.
[24] S. P. Timoshenko and J. M. Gere, *Theory of Elastic Stability*, 2nd ed. New York: McGraw-Hill, 1961.
[25] S. Uma, A. D. McConnell, M. Asheghi, K. Kurabayashi, and K. E. Goodson, "Temperature-dependent thermal conductivity of undoped polycrystalline silicon layers," *Int. J. Thermophys.*, vol. 22, no. 2, pp. 605–616, Mar. 2001.
[26] W. N. Sharpe, K. J. Hemker, K. M. Jackson, and Z. Xie, "Effect of specimen size on Young's modulus and fracture strength of polysilicon," *J. Microelectromech. Syst.*, vol. 10, no. 3, pp. 317–326, Sep. 2001.
[27] M. Zalalutdinov, A. Olkhovets, A. Zehnder, B. Ilic, D. Czaplewski, and H. G. Craighead, "Optically pumped parametric amplification for micromechanical oscillators," *Appl. Phys. Lett.*, vol. 78, no. 20, pp. 3142–3144, May 2001.
[28] Q. Huang, G. Xu, L. Qi, and W. Li, "A simple method for measuring the thermal diffusivity of surface-micromachined polysilicon thin films," *J. Micromech. Microeng.*, vol. 16, no. 5, pp. 981–985, May 2006.
[29] H. S. Carslaw and J. C. Jaeger, *Conduction of Heat in Solids*, 1st ed. London, U.K.: Oxford Univ. Press, 1947.
[30] E. Doedel, H. Keller, and J. Kernevez, "Numerical analysis and control of bifurcation problems, Part I: Bifurcation in finite dimensions," *Int. J. Bifur. Chaos*, vol. 1, no. 3, pp. 493–520, 1991.
[31] E. Doedel, H. Keller, and J. Kernevez, "Numerical analysis and control of bifurcation Problems, Part II: Bifurcation in infinite dimensions," *Int. J. Bifur. Chaos*, vol. 1, no. 4, pp. 745–772, 1991.
[32] J. Guckenheimer and P. Holmes, *Nonlinear Oscillations, Dynamical Systems and Bifurcations of Vector Fields*. New York: Springer-Verlag, 1996.
[33] M. Zalalutdinov, J. W. Baldwin, M. H. Marcus, R. Reichenbach, J. Parpia, and B. Houston, "Two-dimensional array of coupled nanomechanical resonators," *Appl. Phys. Lett.*, vol. 88, no. 14, p. 143 504, Apr. 2006.
[34] M. Pandey, K. Aubin, M. Zalalutdinov, R. B. Reichenbach, A. Zehnder, R. H. Rand, and H. G. Craighead, "Analysis of frequency locking in optically driven MEMS resonators," *J. Microelectromech. Syst.*, vol. 15, no. 6, pp. 1546–1554, Dec. 2006.
[35] M. Pandey, R. H. Rand, and A. T. Zehnder, "Perturbation analysis of entrainment in a micromechanical limit cycle oscillator," *Commun. Nonlinear Sci. Numer. Simul.*, vol. 12, no. 7, pp. 1291–1301, Oct. 2007.

Tuhin Sahai received the B.S. and M.S. degrees in aerospace engineering from the Indian Institute of Technology Bombay, Mumbai, India, in 2002, and the Ph.D. degree from the Department of Theoretical and Applied Mechanics, Cornell University, Ithaca, NY, in 2008.

He is currently a Research Scientist with the United Technologies Research Center, East Hartford, CT.

Alan T. Zehnder received the B.S. degree in mechanical engineering from the University of California, Berkeley, in 1982, and the Ph.D. degree from the California Institute of Technology, Pasadena, in 1987.

He is a Professor with the Department of Theoretical and Applied Mechanics and with the Sibley School of Mechanical and Aerospace Engineering, Cornell University, Ithaca, NY. He has held visiting positions at the Naval Surface Warfare Center, the California Institute of Technology, and the Technical University of Vienna, Vienna, Austria. His research interests are in experimental mechanics, fracture, mechanics of materials, thermomechanical couplings in solids, and micromechanical/nanoelectromechanical system dynamics.